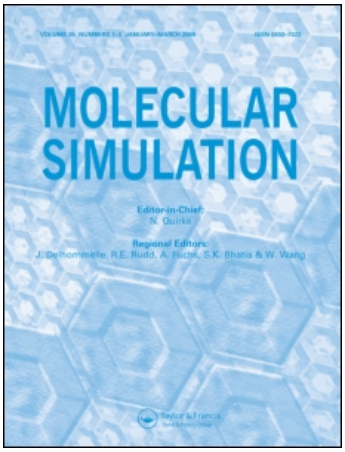


**Molecular Simulation**
Publication details, including instructions for authors and subscription information:
http://www.informaworld.com/smpp/title~content=t713644482

# The effects of nanotube fillers on craze formation in simulated glassy polymers under tensile load

D. G. Richardson[a]; C. F. Abrams[b]
[a] Department of Chemical and Biological Engineering, Drexel University, Philadelphia, PA, USA [b] Department of Computer Science, Drexel University, Philadelphia, PA, USA

**To cite this Article** Richardson, D. G. and Abrams, C. F.(2007) 'The effects of nanotube fillers on craze formation in simulated glassy polymers under tensile load', Molecular Simulation, 33: 4, 421 — 427
**To link to this Article: DOI:** 10.1080/08927020601154637
**URL:** http://dx.doi.org/10.1080/08927020601154637

*Molecular Simulation*, Vol. 33, Nos. 4–5, 15–30 April 2007, 421–427

Taylor & Francis
Taylor & Francis Group

# The effects of nanotube fillers on craze formation in simulated glassy polymers under tensile load

D. G. RICHARDSON‡ and C. F. ABRAMS†*

†Department of Chemical and Biological Engineering, Drexel University, Philadelphia, PA 19104, USA
‡Department of Computer Science, Drexel University, Philadelphia, PA 19104, USA

*(Received June 2006; in final form December 2006)*

We consider the work required to deform uniformly dense polymer systems of glassy bead-spring chains filled with rod-like inclusions with aspect ratio akin to carbon nanotubes (CNTs). We consider 0, 0.40, and 2.0 wt% of filler particles. For each composition, we vary the attractive strength of the polymer–inclusion interaction between one and eight times the nominal polymer–polymer interaction strength. Significant enhancements in plateau stress and work of deformation are observed only for the highest weight fraction of the most attractive inclusions. We show that the primitive path algorithm can be used in polymer glasses to simplify the identification of entanglements. We show that the number of entanglements and chains bridging multiple inclusions cannot be directly used to predict the toughness of the polymer composite. Our results indicate that entanglements do not appear to be the primary molecular-scale structural features responsible for determining material properties of polymer glasses.

*Keywords*: Polymer; Glass; Nanocomposite; Simulation; Molecular dynamics; Deformation



## 1. Introduction

Filler particles have the potential to alter the material properties, such as toughness, of polymeric materials. The exact mechanisms of this alteration are poorly understood. Here, we explore the hypothesis that alteration of the entanglement network by fillers can lead to changes in material toughness. For several years, carbon nanotubes (CNTs [1]) have been suggested as the ultimate filler particle for polymers [2–4]. Because of their high-aspect ratio, CNTs can themselves entangle with polymer chains if the chains wind about the CNTs. There is both experimental [5] and simulation evidence [6,7] that polymers wind about CNTs, offering the possibility that the typical entanglement network in a glass filled with CNTs can differ significantly from that in a neat glass.

Dense systems of flexible polymers at concentrations above the so-called overlap threshold exist as entangled networks of chains [8]. Entanglements are thought of as topological features of the polymer network that restrict polymer motion. This restriction of motion is the result of the inability of polymer chains to cross each other without breaking bonds. As elements in models of melt and solution rheology, entanglements have proven useful; it is interesting, therefore, to speculate on what role they may play in determining the material properties of polymeric glasses. The entanglement network is believed to be responsible for the toughness of polymeric materials, primarily because polymeric solids craze significantly under tensile load prior to failure and the fibril spacing and diameters of crazes have been linked to the entanglement molecular weight [9–12].

Recently, there has been interest in investigating the work required to grow a craze in entangled [10] and cross-linked [11,12] generic bead-spring polymer glasses using non-equilibrium molecular dynamics (MD) simulations. Using properties of crazes determined through molecular simulations, a model has been developed to predict the macroscopic fracture energy of amorphous glassy polymers [13]. There have as yet been no systematic simulation-based studies of entanglements in filled polymer glasses. There has been some interest [14–16] in confined polymer systems similar to the ones we consider in this paper. However, the focus of such previous work has been on the melt structure of the polymer near the surface, not on the toughness of the system under tensile load nor on the possible role of entanglements.

*Corresponding author. Email: cfa22@drexel.edu

*Molecular Simulation*
ISSN 0892-7022 print/ISSN 1029-0435 online © 2007 Taylor & Francis
http://www.tandf.co.uk/journals
DOI: 10.1080/08927020601154637

The purpose of this paper is to investigate any link between entanglements and toughness in filled polymer glasses using a combination of non-equilibrium MD simulations and primitive path analyses. Our methods are similar to those employed for investigating the toughness of entangled and cross-linked systems [10–12]. With respect to those previous studies, we make the following contributions: (a) we consider the effects of CNT-like inclusions (b) and we use the primitive path algorithm [17,18] to show the evolution of the entanglement network of the polymer glass while it is under tensile load, and (c) we help to elucidate the role of the entanglement network in the crazing of polymers. We assess the effects of inclusion composition and polymer–inclusion interaction strength on both the numbers and distributions of entanglements and on material properties. Figure 1 displays snapshots from a typical MD simulation as well as their primitive path counterparts.

## 2. Simulation methods

### 2.1. Model

The prototypical system in this study is a dense glass of bead-spring polymer chains filled with stiff rod-like bead-spring inclusions and confined between two impenetrable walls placed perpendicular to the $z$-axis. Periodic boundaries are applied in the $x$ and $y$ directions. The system contains two types of particles: polymer monomers and inclusion monomers; both are treated as point masses. The interaction potentials and potential parameters for all pairs of monomer types are selected such that the monomers are spherically symmetric with a diameter of $1\sigma$. Reduced units are used throughout. $\epsilon$ is the base unit for energy, $\sigma$ is the base unit for length, $m = 1$ is the base unit for mass and $\tau = \sigma\sqrt{m/\epsilon}$ is the base unit for time.

MD with a Langevin thermostat is employed to generate glass configurations. MD numerically solves Newton's equations of motion for each particle; particles interact according to a potential energy function, $U$. We employ a set of potentials to model the polymer chains which are standard for dense bead-spring melts and glasses. The bonded interactions along both the polymer chains and the inclusions are modeled via the finitely extensible non-linear elastic (FENE) potential: [19]

$$U_{\mathrm{FENE}}(r_{ij}) = -\frac{1}{2}\epsilon a R_0^2 \ln\left[1 - \left(\frac{r_{ij}}{R_0}\right)^2\right] \tag{1}$$

where $a$ is a parameter representing bond strength, $R_0$ is a parameter representing the equilibrium bond distance and $r_{ij}$ is the scalar distance between monomers $j$ and $i$. We use standard parameters of $a = 30$ and $R_0 = 1.5$ which effectively render impossible the crossing of bonds. [19]

For polymer chains and inclusions, monomer–monomer excluded volume between bonded monomers is modeled via the fully repulsive (a.k.a. "athermal") Weeks–Chandler–Andersen (WCA) potential: [20]

$$U_{\mathrm{WCA}}(r_{ij}) = \begin{cases} 4\epsilon\left[\left(\frac{\sigma}{r_{ij}}\right)^{12} - \left(\frac{\sigma}{\mathbf{r}_{ij}}\right)^{6} + \frac{1}{4}\right], & r_{ij} < 2^{1/6}\sigma \\ 0, & r_{ij} \geq 2^{1/6}\sigma \end{cases} \tag{2}$$

For the inclusions, stiffness is modeled using the harmonic spring potential:

$$U_{\mathrm{angle}}(\theta_{ijk}) = 5\epsilon(\theta_{ijk} - \pi)^2 \tag{3}$$

where monomer $i$ is bonded to monomer $j$, monomer $j$ is bonded to monomer $k$, $b_{ji}$ is the vector from $i$ to $j$, $b_{jk}$ is the vector from $k$ to $i$ and $\theta_{ijk}$ is the angle between $b_{ji}$ and $b_{jk}$.

For the simulations, the interaction between polymer and inclusion monomers is made attractive to varying degrees using a standard truncated and shifted Lennard–Jones (LJ) potential with the well depth labeled as $b$:

$$U_{\mathrm{LJ}}(r_{ij}) = \begin{cases} 4b\epsilon\left[\left(\frac{\sigma}{\mathbf{r}_{ij}}\right)^{12} - \left(\frac{\sigma}{\mathbf{r}_{ij}}\right)^{6} - U_{\mathrm{sLJ}}\right], & r_{ij} < 2.5\sigma \\ 0, & r_{ij} \geq 2.5\sigma \end{cases} \tag{4}$$

where $U_{\mathrm{sLJ}} = (\sigma/2.5)^{12} - (\sigma/2.5)^6$. Intermolecular interactions between chain–chain and inclusion–inclusion monomer pairs use equation (4) with $b = 1$. Simulations are conducted for $b = 1$, 2, 4 and 8 with inclusion wt% of 0.10, 0.40 and 2.0. These wt% correspond to the limiting case of a single dilute inclusion, inclusions separated by more than the unperturbed bulk chain radius of gyration

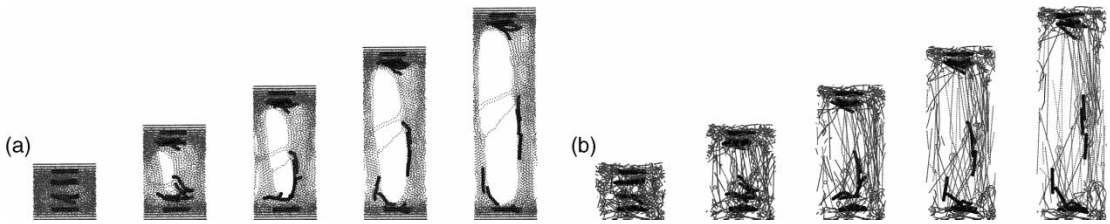


Figure 1. Snapshots from a MD simulation of a glassy polymer (gray) with 2.0 wt% of stiff filler particles (black) confined between two attractive walls for (a) the MD configuration and (b) the corresponding primitive path. The bottom wall is immobile and the top wall is being pulled upwards at a constant velocity.

($R_g = 5.24\sigma$), and inclusions separated by less than the unperturbed bulk chain radius of gyration. For comparison, neat glasses are also simulated. Three independent runs of both neat glass and each combination of $b$ and weight fraction are considered.

The walls are modeled using the two-dimensional analogue of the LJ potential:

$$U_w(r_{iw}) = \begin{cases} \frac{100}{3}\epsilon\left[\left(\frac{2\sigma_w}{5r_{iw}}\right)^{10} - \left(\frac{2\sigma_w}{5r_{iw}}\right) - U_{ws}\right], & r_{iw} < 2.5\sigma_w \\ 0, & r_{iw} \geq 2.5\sigma_w \end{cases} \quad (5)$$

where $\sigma_w = 1$ is the thickness of the wall, $r_{iw}$ is the scalar distance of closest approach between monomer $i$ and the wall and

$$U_{ws} = \left(\frac{2}{5}\cdot\frac{2.5\sigma_w}{w_c}\right)^{10} - \left(\frac{2}{5}\cdot\frac{2.5\sigma_w}{w_c}\right)^{4}$$

.

The monomers in the simulation domain are evolved through time using the velocity-Verlet leap-frog integrator [21] with a time step of 0.01. The walls are evolved through time using the instantaneous force on each wall and a time step of 0.01.

All tensile-failure simulations are conducted in the *NVT* ensemble using a Langevin thermostat [22] with a friction of 0.5 and a setpoint temperature of $T = 0.33$. Monomer–monomer pairwise interactions are identified using the combined neighbor list and cell list method [22].

### 2.2. Simulation protocol

For each simulation, $M = 100$ polymer chains of length $N = 100$ are randomly placed in the simulation domain. The simulation domain is initially cubic and sized such that the monomer density is $\rho = 0.85$ at melt conditions. This results in an edge length of $22.74\sigma$. Prior to the introduction of the walls, periodic boundaries are applied in $x$, $y$ and $z$. Bonded monomers are placed with an initial separation corresponding to the equilibrium FENE bond distance (i.e. the magnitude of separation where the FENE potential is at a minimum). Each polymer monomer is assigned a random velocity drawn from an exponential distribution with mean 1.0. Inclusions of length $N_i = 10$ are placed with all 1–2–3 bond angles set to $\pi$ and parallel and centered on the $z$-axis of the primary simulation domain. The inclusions are placed on a regular square lattice parallel to and centered on the $xy$-plane of the primary simulation domain. The lattice spacing $L$ is the largest value for which (a) the inclusions fit into the simulation domain and (b) the periodic images of the inclusions form a regular square lattice with spacing $L$. Inclusion monomers are effectively initially given an infinite mass by having the integrator skip them.

This initialization procedure results in significant particle overlaps. To remove these overlaps, the simulations are warmed up with 10,000 steps during which the non-bonded particle interactions are described by a radially shifted WCA potential to reduce the forces to magnitudes that could be simulated without loss of stability. The strength of the magnitude of the radial shifting was linearly decreased each time step until at the end of the warmup the non-bonded particle excluded volume interactions had reached full strength [23]. The Langevin thermostat is not yet engaged and velocities are rescaled and shifted so the average per particle kinetic energy was 1.0 and there is no center of mass velocity drift. After the warmup, the confinement phase of the simulation begins.

The well depth of the inclusion–polymer interaction potential is set to $b = 1$ and all potentials are as described in Section 2.1. The periodic boundary in $z$ is disabled and the $z$-coordinates of each particle are appropriately unfolded. Periodic boundaries are retained in $x$ and $y$. The walls are then placed perpendicular to the $z$-axis with one wall at the bottom of the simulation domain and the other at the top. The distance between the walls is reduced by $0.01\sigma/\tau$ until the particle density between the walls is 0.85. This rate of contraction is slow enough to prevent any particles from "escaping" the walls. The walls are then given an effectively infinite mass by having the integrator skip them. After the particles are confined between the walls, the equilibration phase of the simulation begins.

The equilibration time, $\tau_e$, is defined as the time required on average for chains to diffuse a distance equal to their own radii of gyration. We have previously shown that for $N = 100$ that $\tau_e < 25,000$ [7]. The Langevin thermostat is applied with a set temperature of $T = 1.0$. All simulations are equilibrated for $25,000\tau$. After the chains are equilibrated, the quench phase of the simulation begins.

The walls are given a mass of twice the wall area and allowed to move along $z$. The well depth $b$ is set to its final value and the simulation is conducted for $2000\tau$. The simulation is then conducted for a sequence of $2000\tau$ intervals where the set point temperature is reduce to $T = 0.7$, 0.5 and 0.33. The result is a uniformly dense glassy system with a density above the Sastry density [24,25]. Below the Sastry density, there is a glass–gas mechanical instability that does not allow for uniform polymer density. For the 2.0 wt% systems, quenching with $b > 1$ resulted in void formation. For these systems, the simulation was quenched using $b = 1$ and $b$ was set to its final value after the quench.

After the quench, tensile testing begins. The bottom wall is given infinite mass. The top wall is then pulled up at a constant velocity of $0.03\sigma/\tau$ for $2000\tau$. To investigate the effect of inclusion stiffness and connectivity, tensile tests are performed for the following cases (a) inclusions are modeled as described in Section 2.1, (b) the inclusion angle potential is turned off and (c) the inclusions are dissociated.

### 2.3. Observable definitions

Strain is computed as $(E - E_0)/E_0$ where $E$ is the distance between the walls and $E_0$ is the distance between the walls at the end of the quench phase of the simulation immediately prior to initiating the deformation. The force on the top wall in the $z$-direction, $F$, is the opposite of the $z$-direction forces experienced by all particles interacting with the wall. Stress is computed as $F/A_w$ where $A_w$ is the wall area. The work required to deform the system to a given extension $E$, is computed as

$$W = \int_{x=E_0}^{E} F \, dx. \tag{6}$$

Distance $E$ and force $F$ are sampled at the highest possible frequency, i.e. once per time step and $W$ is computed by numerical integration.

The primitive path analysis (PPA) algorithm [17,18] is used to simplify the detection of entanglements. The PPA algorithm is applied to a simulation configuration by (a) giving all chain ends an infinite mass, (b) disabling intramolecular excluded volume, (c) setting $b = 1$ and (d) driving the system to zero temperature. To prevent instability due to the sudden loss of intramolecular excluded volume, the PPA is conducted in a strong thermostat phase and a weak thermostat phase. We use a set-point temperature of 0.001. Using the rigorous equilibration criteria presented in Ref. [18] would make it computationally infeasible to apply PPA to multiple configurations during tensile failure. Because of this, our strong-thermostat phase is conducted with a friction of 50 for $50\tau$ and our weak thermostat phase is conducted with a friction of 0.5 for $450\tau$. These time scales are sufficient to detect the evolution of the entanglement network during tensile deformation.

In the absence of entanglements, PPA contracts all chains to straight lines because the FENE potential has a minimum at a separation distance of zero. Because the combination of intermolecular excluded volume and the FENE potential prevent chain crossing, chains that are entangled will be both touching and curved about each other. We consider an entanglement to be 10 or more consecutive monomers with a curvature of at least 0.75 and the entanglement owner to be the monomer in the entanglement with the highest curvature. This definition of entanglement is similar in spirit to the definition used in Ref. [26] to locate entanglements in a PPA configuration confined to a lattice. We classify an entanglement as an inclusion–chain entanglement if there is an inclusion monomer within 1.5 of the entanglement owner. Otherwise, the entanglement is classified as a chain–chain entanglement.

To quantify the number of chains interacting with more than one inclusion, we define the chain–inclusion contact number $C$ of a chain to be the number of inclusions for which the chain has at least one chain monomer within $1.5\sigma$ of at least one of the inclusion's monomers. We classify a chain to be a bridging chain if in the PPA, the $C$ of the chain is greater than 1.

## 3. Results and discussions

Motivated by the propensity for chains to wind about cylindrical inclusions and thereby alter the entanglement network of a polymer melt [7], we began our investigation with a polymer–inclusion well depth of $b = 1$. Because, $b = 1$ causes all LJ pair interactions to be equivalent, any additional work required to deform a filled glass must arise solely from the changes the inclusions cause in the entanglement network or, by virtue of the inclusion stiffness, increased work required to move the inclusion monomers relative to polymer monomers. For the wt% considered and $b = 1$, there is no increase in the work (see figure 2(a)) required to deform each glass. During the deformation, the number of entanglements decreases only slightly (see figure 4(a)). Additionally, the number of entanglements for the filled glasses is always about 10% less than is observed in the neat glass. Low wt% of the inclusions with inclusion

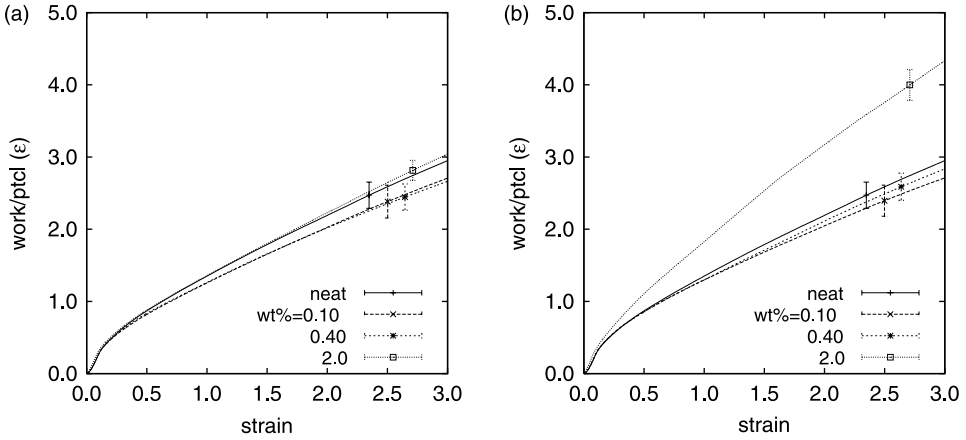


Figure 2. Effect of filler composition on work of deformation in the tensile deformation of a polymer glass. Work (normalized by number of particles) vs. strain for various wt% of stiff inclusions of length 10. Polymer–tube interaction well-depth is (a) $b = 1\epsilon$ and (b) $8\epsilon$.

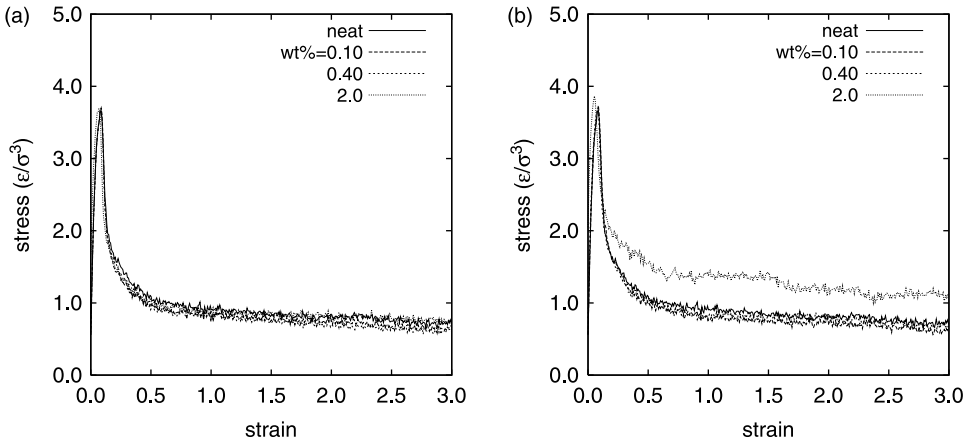


Figure 3. Effect of filler composition on stress–strain behavior in the tensile deformation of a polymer glass. Stress vs. strain for various wt% of stiff inclusions of length 10. Polymer–tube interaction well-depth is (a) $b = 1\epsilon$ and (b) $8\epsilon$.

monomers that are thermodynamically equivalent to polymer monomers are clearly incapable of providing an increase in material toughness or significantly altering the number of entanglements. They also did not alter the distribution of work between the energy needed for plastic and elastic deformation or alter the yield point of the material (see figure 3(a)).

To investigate the effect of increased attraction between the polymer and inclusion monomers, we considered $b = 2$, 4 and 8. At each filler wt% for both $b = 2$ and 4 (not shown), there was no difference in the work required or number of entanglements relative to $b = 1$.

However, for $b = 8$, we observe an increase of more than 20% in the work required to deform a glass with 2.0 wt% inclusion (see figure 2(b)). Even with $b = 8$, wt% below 2.0% did not show an increase in the work required to deform the sample (see figure 2(b)). Nearly all of this increase in work of deformation occurred during plastic deformation of the glass and did not dramatically alter the yield point of the glass. As shown in figure 3(b), the only conditions under which the plateau stress is significantly higher are those at the highest inclusion wt% and highest polymer–inclusion interaction strength. Importantly, the increase in work occurred with both fewer entanglements than the neat glass and roughly the same number of entanglements as the other filled glasses, as shown in figure 4(b).

Clearly, the number of entanglements is not the only factor governing the work required to deform a glass. In an attempt to distinguish between different kinds of entanglements, we looked into the distribution of entanglements between chain–chain and chain–inclusion entanglements (see figure 5). The number of chain–inclusion entanglements are only about 10% of the total number of entanglements and their number remains almost constant throughout the deformation.

Once the polymer composites are equilibrated and quenched, the stiffness and connectivity of the inclusions have little impact on the work required to deform the glass as shown in figure 6. However, because the inclusions are both connected and stiff during preparation of the glass, it is possible a memory effect imparts the enhance material toughness when the inclusions are flexible and dissociated.

It is also interesting that the increase in toughness happens only for the combination of $b = 8$ and 2.0 wt% of inclusion. At this wt%, the inclusion lattice spacing is less

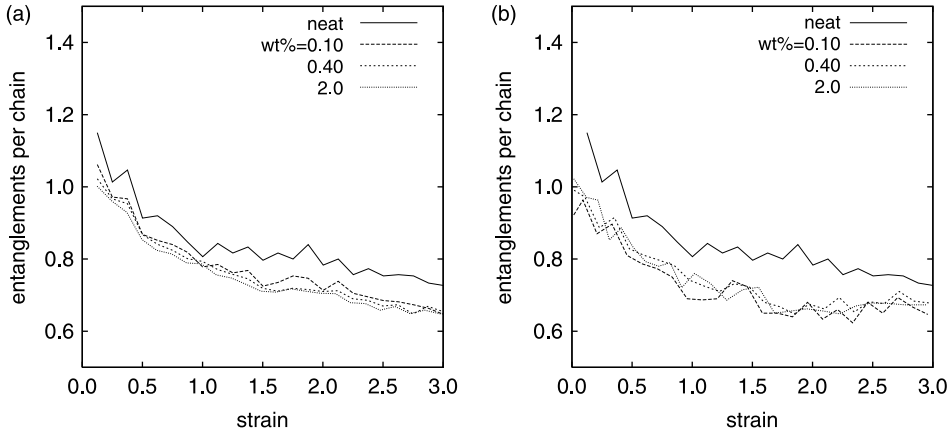


Figure 4. Effects of filler composition and strain on the number of entanglements in the tensile deformation of a polymer glass. Average number of entanglements per chain vs. strain for various wt% of stiff inclusions of length 10. Polymer–tube interaction well-depth is (a) $b = 1\epsilon$ and (b) $8\epsilon$.

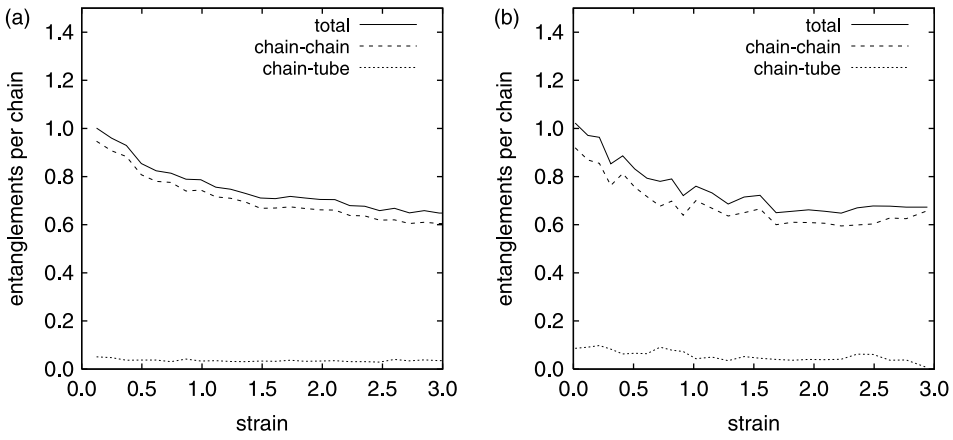


Figure 5. Effect of polymer–tube interaction well-depth on the evolution of chain–chain and chain–tube entanglements in the tensile deformation of a polymer glass. Polymer–tube interaction well-depth is (a) $b = 1\epsilon$ and (b) $8\epsilon$.

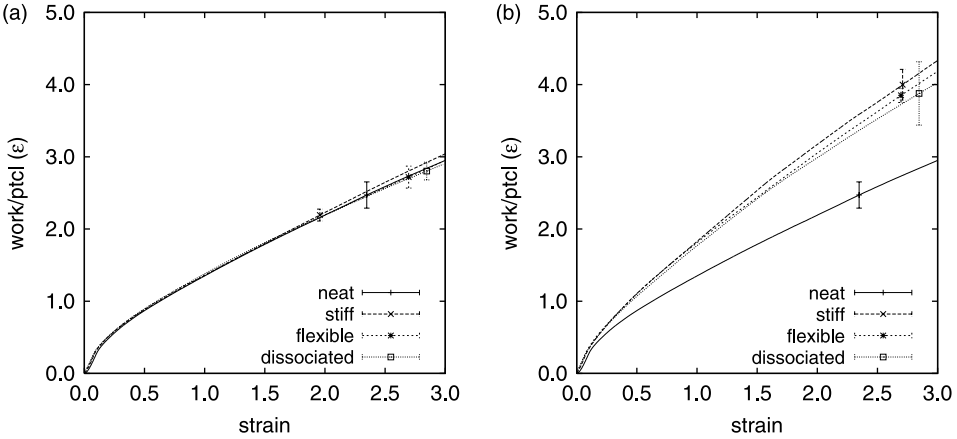


Figure 6. Effect of inclusion flexibility and connectivity on work of deformation. Work vs. strain for tensile deformation of glasses of 100 chains and 20 wt-% length 10 inclusions for which $b = 1\epsilon$. "Stiff" refers to the standard nanotube-like inclusions; "flexible" to inclusions for which no stiffness is employed; "dissociated" for inclusions for which FENE/LJ bonds are turned off prior to deformation.



than the $R_g$ of the bulk polymer. This decrease in lattice spacing results in almost a 12-fold increase in the number of chains interacting with more than one inclusion, as shown in figure 7. However, one should note that the number of bridging chains is not sensitive to the polymer–inclusion interaction strength for $b > 2$.

Therefore, none of (i) the number of entanglements, (ii) their distribution between the chain–chain and chain–inclusion entanglements, or (iii) the percentage of bridging chains is sufficient to account for the amount of work required to deform the glass. It is possible that some entanglements confer more toughness than others. This could be due to the orientation of the entanglement relative to the pulling axis or because some entanglements are more topologically constraining than others. It is also possible that during the pull existing entanglements are constantly being unformed while new entanglements are formed. In this situation, the lifetime of the entanglements may play a more predictive role than the number of entanglements. We defer investigation of entanglement lifetime and quality to later study. Moreover, because enhanced material toughness is only observed for this higher degree of bridging, we suspect the existence of a critical threshold for the density of rod-like inclusion particles below which there can be no enhanced material toughness as a result of the inclusions.

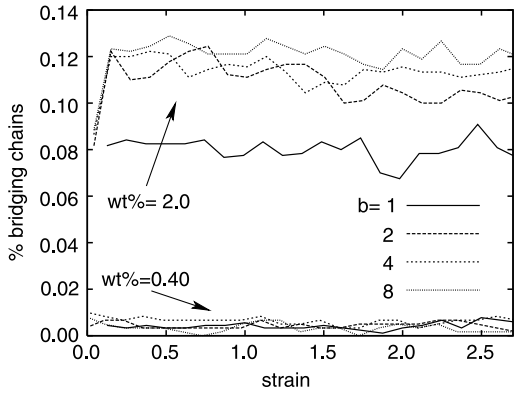


Figure 7. Effect of polymer–tube interaction well-depth on fraction of chains that bridge two tubes. Percentage of bridging chains vs. strain for various polymer–tube interaction well-depths, $b$ and inclusion wt% of 0.4 and 2.0.

## 4. Conclusions

We have successfully developed a metric for measuring the number of entanglements that exist in the primitive path of a polymer. This metric relies on the use of PPA in a glass. It appears to be robust in the face of both traditional MD and the non-equilibrium MD simulation performed to apply tensile load. It also validates that PPA can be used in glasses.

At low wt% of inclusion (less than 0.4 wt-%), we observe no dependence in the toughness of a polymer glass filled with rod-like inclusions when there is a strongly attractive interaction between the inclusion and polymer monomers. At a high inclusion density (2.0 wt-%), we observe more than 20% increase in toughness (at a strain of 2.0) relative to all other cases. We observe that compositions of 0.4 and 2.0 wt-% define a transition between a regime in which chains cannot bridge multiple inclusions and a regime in which they can. We hypothesize that there may exist a critical inclusion density below which stiff rod-like inclusions are incapable of providing an enhancement to a polymer composite which depends on bridging, and current simulations are ongoing to test this hypotheses.

Understanding the mechanism through which these attractive inclusions stabilizes the craze would be of significant practical value to those engineering polymer composites. We have shown that the number of entanglements is insufficient to predict the increase stability of the craze. We are currently planning to investigate both entanglements dynamics and the difference between types of entanglements in an attempt to better understand the essential physics required to stabilize craze formation. We also plan to investigate longer filler particles and larger systems.



## Acknowledgements

Financial support from the United States Office of Naval Research through Award N00014-03-1-0655 is gratefully acknowledged.

## References

[1] S. Iijima. Helical microtubules of graphitic carbon. *Nature*, **354**(6348), 56 (1991).
[2] E.T. Thostenson, Z. Ren, T.-W. Chou. Advances in the science and technology of carbon nanotubes and their composites: A review. *Compos. Sci. Technol.*, **61**(13), 1899 (2001).
[3] K.-T. Lau, M. Chipara, H.-Y. Ling, D. Hui. On the effective elastic moduli of carbon nanotubes for nanocomposite structures. *Compos. Part B Eng.*, **35**(2), 95 (2004).
[4] C. Wang, Z.-X. Guo, S. Fua, W. Wub, D. Zhu. Polymers containing fullerene or carbon nanotube structures. *Prog. Polym. Sci.*, **29**(11), 1079 (2004).
[5] B. McCarthy, A.B. Dalton, J.N. Coleman, H.J. Byrne, P. Bernier, W.J. Blau. Spectroscopic investigation of conjugated polymer/single-walled carbon nanotube interactions. *Chem. Phys. Lett.*, **250**, 27 (2001).
[6] V. Lordi, N. Yao. Molecular mechanics of binding in carbon-nanotube-polymer composites. *J. Mater. Res.*, **15**(12), 2770 (2000).
[7] D.G. Richardson, C.F. Abrams. Polymer chain winding in the melt. *Macromolecules*, **39**(6), 2330 (2006).
[8] P.G. de Gennes. *Scaling Concepts in Polymer Physics*, Cornell university press, Ithaca, New York (1979).
[9] E.J. Kramer. Microscopic and molecular fundamentals of crazing. *Adv. Polym. Sci.*, **52/53**, 1 (1983).
[10] A.R.C. Baljon, M.O. Robbins. Simulations of crazing in polymer glasses: Effect of chain length and surface tension. *Macromolecules*, **34**(12), 4200 (2001).
[11] M.J. Stevens. Interfacial Fracture between Highly Cross-Linked Polymer Networks and a Solid Surface: Effect of interfacial bond density. *Macromolecules*, **34**(8), 2710 (2001).
[12] M. Tsige, M.J. Stevens. Effect of cross-linker functionality on the adhesion of highly cross-linked polymer networks: A molecular dynamics study of epoxies. *Macromolecules*, **37**(2), 630 (2004).
[13] J. Rottler, S. Barsky, M.O. Robbins. Cracks and crazes: On calculating the macroscopic fracture energy of glassy polymers from molecular simulation. *Phys. Rev. Lett.*, **89**(14) (2002) 148304-1–148304-4.
[14] I. Bitsanis, G. Hadziioannou. Molecular dynamics simulations of the structure and dynamics of confined polymer melts. *J. Chem. Phys.*, **92**(6), 3827 (1990).
[15] K.A. Smith, M. Vladkov, J.-L. Barrat. Polymer melt near a solid surface: A molecular dynamics study of chain conformations and desorption dynamics. *Macromolecules*, **38**(2), 571 (2005).
[16] K.C. Daoulas, V.A. Harmandaris, V.G. Mavrantzas. Detailed atomistic simulation of a polymer melt/solid interface: Structure, density, and conformation of a thin film of polyethylene melt adsorbed on graphite. *Macromolecules*, **38**(13), 5780 (2005).
[17] R. Everaers, S.K. Sukumaran, G.S. Grest, C. Svaneborg, A. Sivasubramanian, K. Kremer. Rheology and microscopic topology of entangled polymeric liquids. *Science*, **303**(5659), 823 (2004).
[18] S.K. Sukumaran, G.S. Grest, K. Kremer, R. Everaes. Identifying the primitive path mesh in entangled polymer liquids. *J. Polym. Sci. Pol. Phys.*, **43**, 917 (2005).
[19] K. Kremer, G.S. Grest. Dynamics of entangled linear polymer melts: A molecular-dynamics simulation. *J. Chem. Phys.*, **92**(8), 5057 (1990).
[20] J.D. Weeks, D. Chandler, H.C. Andersen. Role of repulsive forces in determining the equilibrium structure of simple liquids. *J. Chem. Phys.*, **54**(12), 5237 (1971).
[21] W.C. Swope, H.C. Andersen, P.H. Berens, K.R. Wilson. A computer simulation method for the calculation of equilibrium constants for the formation of physical clusters of molecules: Applications to small water clusters. *J. Chem. Phys.*, **76**(1), 637 (1982).
[22] D. Frenkel, B. Smit. *Understanding Molecular Simulation*, 2nd ed., Academic Press, San Diego (2001).
[23] C.F. Abrams, K. Kremer. Effects of excluded volume and bond length on the dynamics of dense bead-spring polymer melts. *J. Chem. Phys.*, **116**(7), 3162 (2002).
[24] S. Sastry. Liquid limits: Glass transition and liquid-gas spinodal boundaries of metastable liquids. *Phys. Rev. Lett.*, **85**(3), 590 (2000).
[25] J. Hernández-Rojas, D.J. Wales. Density effects in a bulk binary Lennard–Jones system. *Phys. Rev. B*, **68** (2003) 144202-1–144202-7.
[26] S. Shanbhag, R.G. Larson. Identification of topological constraints in entangled polymer melts using the bond-fluctuation model. *Macromolecules*, **39**(6), 2413 (2006).